Pergamon

Int. J. Solids Structures Vol. 35, Nos 31–32, pp. 4223–4238, 1998

0020-7683/98 $19.00 + .00

PII: S0020-7683(97)00311-9

INFLUENCE OF FIBER BRIDGING ON STRUCTURAL SIZE-EFFECT

VICTOR C. LI,* Z. LIN and T. MATSUMOTO
Advanced Civil Engineering Materials Research Laboratory, University of Michigan, Ann Arbor MI 48109-2125, U.S.A.

(*Received* 26 *August* 1996; *in revised form* 30 *May* 1997)

Abstract—The size-effect of structural element has been experimentally determined in concrete members under various load types. The importance of size-effect on safe structural design has been well recognized. Theoretical models explaining and predicting size-effect based on fracture mechanics of brittle and quasi-brittle materials have made significant advances in the last decade.

Structural size-effect can be reduced by modifying the crack bridging behavior of concrete. An effective means of controlling the crack bridging law is by fiber reinforcement. Since the bridging law is fundamentally governed by fiber and interface properties, proper materials engineering can lead to effective means of reducing structural size-effect.

This paper studies analytically the effectiveness of fiber bridging on the FRC beam structural size effect, by means of a flexural model which takes into account matrix crack extension and fiber bridging. The flexural strength (MOR) is shown to decrease with beam height following Bazant's Size-Effect Law for ordinary concrete. When fiber bridging is introduced, the MOR is shown to be much less dependent on matrix properties. Instead fiber and interface parameters dominate the MOR of the FRC beam. At the same time, beam height-size-effect on MOR is shown to diminish within the practical range of real structural sizes. The relationships between structural strength MOR, the composite σ–δ bridging relation, the material characteristics length, and the constituent fiber, matrix and interface properties are clarified. A generic size-effect law for FRC beams is obtained. Other related issues such as size-effects on R-curve behavior, critical crack length at MOR, etc., are also studied.

INTRODUCTION

The size-effect of structural element, as one of the most important consequences of fracture mechanics, has been studied both experimentally and theoretically in concrete members over the last decade (e.g., Bazant, 1984, 1987, 1992; Bazant and Kazemi, 1990; Carpinteri, 1989). Knowledge of the size effect is of great importance for the safe design of structures. For brittle materials, the maximum nominal stress size-effect of geometrically similar structure elements (e.g., beams) with initial notches can be most illustratively explained by the following LEFM result:

$$\sigma_N = K_{IC} b^{-1/2} f^{-1}\left(\frac{a_0}{b}\right) \quad \left(\sigma_N \propto \frac{1}{\sqrt{b}}\right) \tag{1}$$

where σ_N is the nominal maximum stress, K_{IC} is the material fracture toughness, and a_0 and b are the initial crack length and beam height, respectively. In the case of a 3-point bending beam with beam height b, span S and unit thickness (Fig. 1), σ_N and $f(a_0/b)$ are given by (Tada *et al.*, 1985):

$$\sigma_N = \frac{3P_{max}S}{2b^2} \tag{2a}$$

and

* Author to whom correspondence should be addressed.

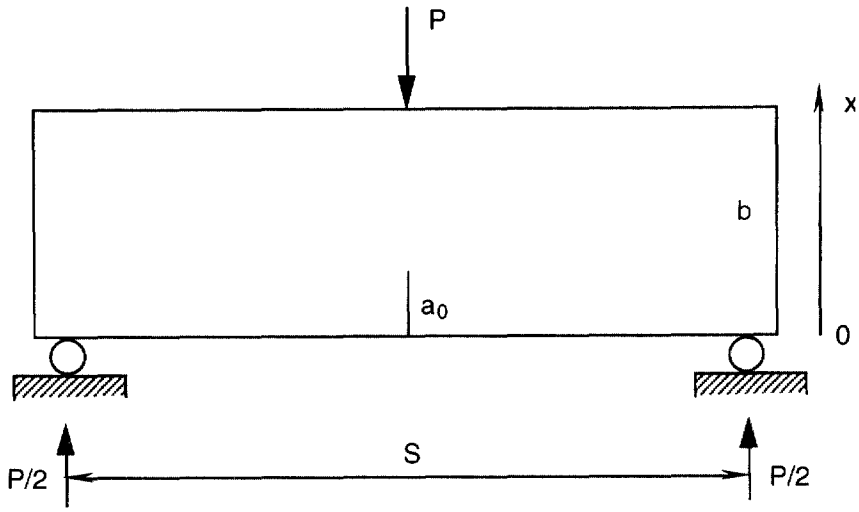

Fig. 1. Geometric and loading configurations of a three-point bending FRC beam.

$$f(\alpha_0) = \alpha_0^{1/2} \frac{1.99 - \alpha_0(1-\alpha_0)(2.15 - 3.93\alpha_0 + 2.7\alpha_0^2)}{(1+2\alpha_0)(1-\alpha_0)^{3/2}}, \quad \alpha_0 = a_0/b \tag{2b}$$

It should be noted that eqn (2b) is given for $S/b = 4$ and any a_0/b. For other S/b ratios, the accuracy of (2b) will slightly decrease.

For quasi-brittle materials, such as concrete, rocks, and fiber-reinforced cement composites, crack extension in a structural element is associated with the growth of fracture process zone (FPZ), the property of which can be characterized by cohesive stress or bridging stress vs crack opening displacement (σ_B–δ) relation (Barenblat, 1962; Hillerborg, 1983). Li and Liang (1986) has demonstrated that the fracture process zone length and the fracture resistance, in general, are not material properties but depends on the geometry of the specimen and the loading configurations. They also concluded that the use of LEFM for crack analysis in concrete and FRC structures are generally invalid unless all relevant structural dimensions are much larger than the steady-state process zone size, and the σ_B–δ relation must be used as a fundamental material property in a nonlinear fracture mechanics analysis.

Without getting into detailed nonlinear fracture mechanics analysis, Bazant and Kazemi (1990) introduced a size-effect law for nominal strength of concrete structures:

$$\sigma_N = C_n \left[\frac{EG_f}{g'(\alpha_0)c_f + g(\alpha_0)b} \right]^{1/2} \tag{3}$$

where G_f and c_f are the fracture energy and the equivalent effective length of fracture process zone for an infinitely large specimen, respectively; $g(\alpha_0) = (C_n f(\alpha_0))^2$ and $C_n = 1.5S/b$ for a three-point bending beam. Equation (3) captures the correct trend of structural size-effect in concrete in a simple, easy-to-use form although it is only approximate due to the truncation of the Taylor series of $g(\alpha)$ in its derivation.

When fibers are introduced, the fracture energy, strength and ductility of an ordinary concrete element can be greatly improved. Fiber reinforcement also adds another dimension to materials engineering in reducing structural size-effect via the control of crack bridging behavior. Furthermore, recent development in FRC structural applications, such as the steel fiber reinforced concrete (SFRC) tunnel linings in Japan (Li, 1995; Nanakorn *et al.*, 1996), posts new challenges in the load-carrying-capacity design for these FRC structures. Predictive capability is certainly needed at both the material and structural level to provide design guidelines in FRC structural applications.

In order to address the above-mentioned issues, quantitative studies explicitly taking into account the FPZ development in FRC structures must be carried out. The crucial information needed will be the crack bridging relation. The crack bridging law as a fundamental material property has been well established in terms of fiber, matrix and interface characteristics, based on micromechanical models of the bridging mechanism of randomly oriented short straight fibers (Li, 1992; Li *et al.*, 1991; Lin and Li, 1997). Further link of those fundamental properties to the structural size-effect through the σ_B–δ relation is needed. Establishing such a link can provide analytic tools for predicting FRC structural load-carrying capacity as well as effective means of reducing structural size-effect through proper materials engineering. In this paper, these issues will be addressed by employing a generic nonlinear fracture mechanics formulation. A three-point bending model which takes into account matrix crack extension and fiber bridging is considered. The relationships between the structural nominal flexural strength (MOR), the composite σ_B–δ bridging relation, the material characteristics length, and the constituent fiber, matrix and interface properties are clarified. A generic size-effect law for FRC beams is obtained. The influence of fiber bridging on the size-effects of *R*-curve behavior and critical crack length at MOR are also analyzed.

APPROACH

In this section, a generic nonlinear fracture mechanics formulation is presented. Based on this formulation, numerical simulations can be performed to obtain the flexural loading associated with matrix crack extension with fiber bridging in a three-point bending FRC beam. Detailed crack opening profiles and bridging stress distributions in the fracture process zone can be computed as well.

Formulation

Figure 1 shows an initially notched three-point beam under mid-span point loading. The load carrying capacity of the FRC beam is assumed to be controlled by the cracking and bridging actions that take place at the mid-span cross-section. A bridged crack model with stress singularity ahead of the fracture process zone is used (see Fig. 2) (Jenq and Shah, 1985; Foote *et al.*, 1986; Cox and Marshall, 1991). The use of a singular model will lead to realistic predictions of crack opening profiles and near-tip deformations (Gettu and Shah, 1994).

Following the standard derivation outlined in Cox and Marshall (1991), the singular integral equation governing the crack opening profile $\delta(x)$ coupled with applied flexural stress $\sigma_a(x)$ and bridging stress $\sigma_B(\delta(x))$ is given by

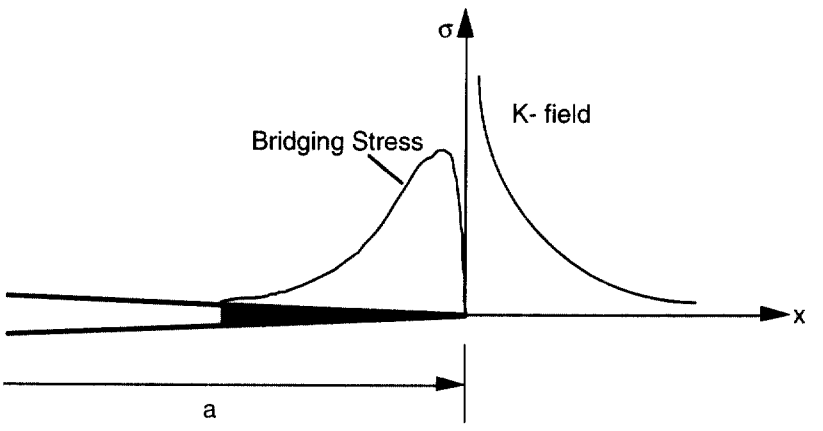

Fig. 2. The bridged crack model.

$$\delta(x) = \frac{8}{E'}\int_x^a \left\{\int_0^{a'} G(x', a', b)[\sigma_a(x') - \sigma_B(\delta(x'))]\,\mathrm{d}x'\right\} G(x, a', b)\,\mathrm{d}a' \tag{4}$$

where E' is the composite Young's modulus ($E' = E$ for plane stress and $E' = E/(1-\nu^2)$ for plane strain); $\sigma_a(x) = \sigma_a(0)(1-2x/b)$, $\sigma_a(0) = (3PS/2b^2)$ for three-point bending case; the weight function $G(x, a, b)$ is given in the Appendix. Based on the superposition scheme, the crack-tip stress intensity factor K_{tip} is given by

$$K_{tip} = K_a + K_B = 2\int_0^a G(x, a, b)[\sigma_a(x) - \sigma_B(\delta(x))]\,\mathrm{d}x \tag{5}$$

Upon crack extension, K_{tip} should be equal to the matrix toughness K_m. This gives an additional equation for solving the applied load required for crack extension in (4), i.e.,

$$2\int_0^a G(x, a, b)[\sigma_a(x) - \sigma_B(\delta(x))]\,\mathrm{d}x = K_m \tag{6}$$

In (4)–(6), the fundamental material property required is the crack bridging relation $\sigma_B(\delta(x))$. Li (1992) has theoretically derived an expression for such a bridging law of tension-softening type for randomly oriented short straight fiber reinforced composites, and it is given by

$$\sigma/\sigma_0 = [1 - \delta/(L_f/2)]^2 \tag{7}$$

where $\sigma_0 = \frac{1}{2}gV_f\tau(L_f/d_f)$ is the maximum bidging stress; V_f, L_f and l_f are the fiber volume fraction, fiber length and fiber diameter, respectively; τ is the interface frictional stress and g is the snubbing factor related to the angle effect when a fiber is pulled out at an inclined angle relative to the loading axis (Morton and Groves, 1976; Li *et al.*, 1990). It should be noted that the crack bridging associated with fiber debonding process is ignored here based on the consideration that in both laboratory-size and real-size structures, the crack opening is generally large enough to get into the tension-softening range at maximum applied or failure load. The fracture energy associated with (7) can be found by integrating the area under the curve shown in Fig. 3 as follows

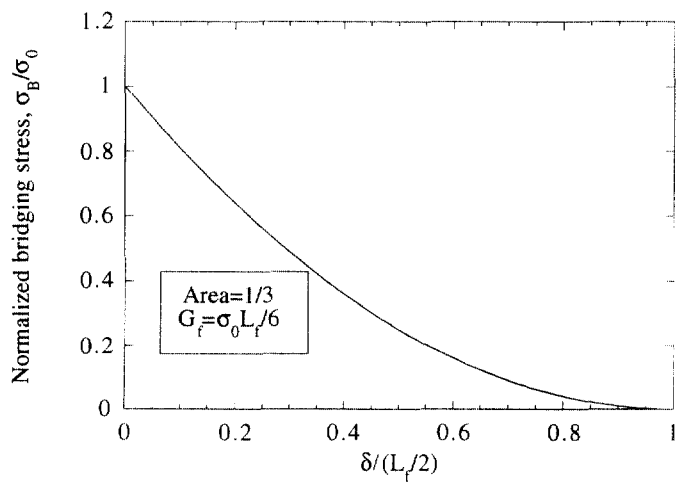

Fig. 3. Non-dimensional tension-softening crack bridging law.

$$G_f = \sigma_0 L_f/6 \tag{8}$$

Both (7) and (8) have been compared with experimental data for steel-fiber and synthetic-fiber reinforced cementitious composites of widely varying micromechanical parameters, and good agreements were found (see Li, 1992 for detail).

Equations (4) and (6) can be re-written in the following non-dimensional form by using σ_0 and $L_f/2$ as normalization factors for stress and length quantities, respectively. That is

$$\tilde{\delta}(X) = S_a A \int_X^1 \left\{ \int_0^t G(s, t, B)[\Sigma(X) - \Sigma_B(\tilde{\delta}(X))]\, ds \right\} G(X, t, B)\, dt \tag{9}$$

and

$$\frac{K_m}{\sigma_0\sqrt{\pi l_{ch}}} = S_a\sqrt{A}\frac{2}{\pi}\int_0^1 G(s, 1, B)[\Sigma(X) - \Sigma_B(\tilde{\delta}(X))/S_a]\, ds \tag{10}$$

where

$$l_{ch} = \frac{\pi E' L_f}{16\sigma_0} = \text{Material characteristic length} \tag{11}$$

$$S_a = \sigma_a(0)/\sigma_0 = \text{Normalized nominal flexural stress amplitude} \tag{12}$$

$$A = a/l_{ch} = \text{Normalized crack length} \tag{13}$$

$$B = b/l_{ch} = \text{Normalized beam height} \tag{14}$$

$$\Sigma(X) = 1 - 2X\frac{A}{B}\,(X = x/a) = \text{Applied load pattern} \tag{15}$$

$$\Sigma_B(\tilde{\delta}(X)) = \frac{\sigma_B}{\sigma_0} = [1 - \tilde{\delta}(X)]^2 = \text{Normalized bridging law} \tag{16}$$

The material characteristic length l_{ch} defined in (11) results from the normalization procedure and could be interpreted as proportional to the ratio of E' to the approximate post-peak softening rate $\sigma_0(L_f/2)$. Combining (8) and (11), l_{ch} can be also written as

$$l_{ch} = \frac{3\pi E' G_f}{8\sigma_0^2} \tag{17}$$

which is similar to that defined in Hillerborg (1983) and Li and Liang (1986). The quantity $B = b/l_{ch}$ is defined as normalized beam height, and it also indicates the structural brittleness as will be seen shortly. One may regard this quantity as the brittleness number.

The numerical scheme for solving equations (9) and (10) to find the nondimensional applied load amplitude S_a along with crack opening profiles for gradually increasing crack lengths has been documented in Cox and Marshall (1991), to which readers are referred for details. The maximum value of S_a gives the normalized nominal flexural strength (MOR) σ_N/σ_0. From the above formulation, it can be concluded that

Table 1. Parameter ranges identified in the present study

Parameter	Range	Note
Initial flaw a_0/b	1–2%	Initial material defect (assumed)
	10–30%	Notched specimens for size-effect study[a]
Material characteristic length l_{ch}	10^{0}–10^{1} m[b]	$l_{ch} = (\pi E L_f/16\sigma_0)$
Brittleness number $B = b/l_{ch}$	10^{-1}–10^{2}	b (real): 10^{-2}–10^{1} meter[c]
$K^* = (K_m/\sigma_0\sqrt{\pi l_{ch}})$	0.01–0.5[d]	$(K_m/\sigma_0\sqrt{\pi l_{ch}}) = 0.51\sqrt{(G_m/G_f)}$

[a] e.g., Bazant and Pfeiffer (1987), Duda and Konig (1990) and Chern and Tarng (1990).
[b] Ref. Hillerborg (1983). [c] Ref. Okamura and Maekawa (1994).
[d] G_m for cement paste and mortar is on the order of 10^{0} and 10^{1} J/m^2, respectively. G_f for FRCs is up to 10^{4} J/m^2 (Wang *et al.*, 1991).

$$\sigma_N/\sigma_0 = \text{function}\left(B, \frac{K_m}{\sigma_0\sqrt{\pi l_{ch}}}, \frac{a_0}{b}\right) \tag{18}$$

The a_0/b dependence in (18) results from the modification to the bridging stress distribution $\Sigma_B(X)$ in (9) and (10) by setting zero bridging stress along the initially notched (unbridged) section of the crack. The dependence of structural strength σ_N/σ_0 on the brittleness number B and the initial crack size (a_0/b) in FRC beams is analogous to similar dependence for concrete beams. The parameter $K^* = (K_m/\sigma_0\sqrt{\pi l_{ch}})$, however, is unique for FRC beams. K^* can be interpreted as a relative matrix crack tip toughness to the FPZ fiber bridging toughness.

The non-dimensional formulation presented here enables us to obtain a generic size-effect law for FRC beams under flexural loading. Equation (18) also identifies the role of fiber, matrix and interface properties in structural size-effect.

Parameter ranges

Table 1 shows that realistic ranges for the parameters identified in (18). These ranges will be covered in our numerical results presented in the next section.

RESULTS AND DISCUSSIONS

Effect of fiber bridging on failure modes of a FRC beam

Fiber bridging tends to stabilize the extension of matrix cracks. The effect of fiber bridging is analogous to the crack closing action provided by distributed nonlinear springs linking the matrix crack faces. Obviously, the brittle or ductile nature of the failure of a FRC structure is strongly controlled by the quality of those nonlinear springs.

Figure 4 shows typical curves of flexural stress σ_{flex} ($= \sigma_a(0)$) vs crack length a in a normalized form. Given the brittleness number and initial notch, the stability of crack growth is governed by the single parameter K^*. Smaller K^* values correspond to stronger fiber bridging or lower matrix toughness K_m. The $K^* = 0.01$ case shows stable crack growth after it initiates until the flexural strength (MOR) is reached. We shall denote this failure mode as Type II (ductile). For $K^* = 0.05$, crack growth is unstable (flexural stress decreases as the crack propagates) following the initiation, and it starts to become stable when crack size (also, FPZ size) becomes large, at least under displacement controlled condition. But the post-first-cracking flexural stress is still lower than the first cracking stress. The same situation is found in $K^* = 0.1$ case except that there is no stable matrix crack growth at all due to the even poorer crack bridging effect. In the latter two cases, the failure of the FRC beam will be catastrophic (Type I, brittle) if load control is assumed. The flexural strength (MOR) for both cases will be taken at the initiation point, which is essentially controlled by the matrix toughness K_m and initial notch size a_0, and follows the LEFM result (1) with $K_{IC} = K_m$.

It is worth mentioning that the normalization for the flexural stress σ_{flex} is performed according to (1) so that the starting points for all the cases will be the same.

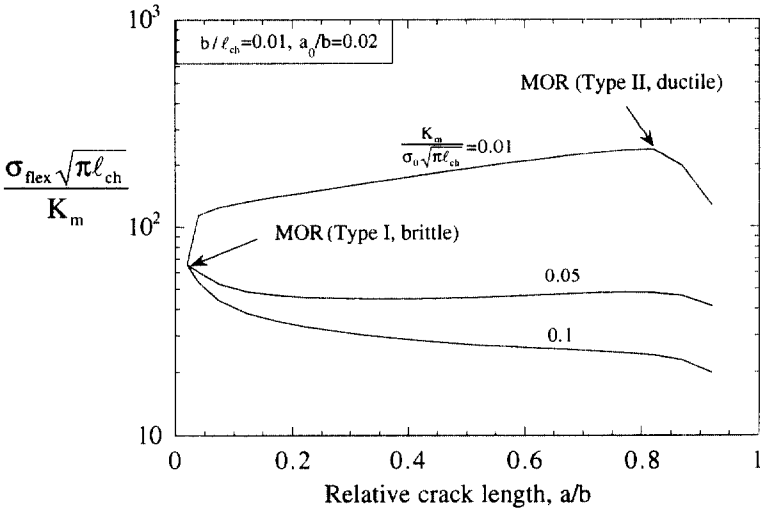

Fig. 4. Normalized flexural stress as a function of relative crack length for $b/l_{ch} = 0.01$ and $a_0/b = 0.02$. The typical ductile failure mode (Type I) and brittle failure mode (Type II) are shown.

Generic size-effect law

It has been shown earlier that the normalized nominal strength of a FRC beam under three-point bending σ_N/σ_0 only depends on three non-dimensional parameters: B, K^*, and a_0/b. In order to obtain such a generic size-effect law, extensive numerical calculations have been carried out. To illustrate, Fig. 5(a)–(h) are presented here corresponding to $a_0/b = 0.01$, 0.02, 0.05, 0.1, 0.2, 0.3, 0.5 and 0.7 cases, respectively. The parallel straight lines or line segments of slope $(-1/2)$ indicate Type I (brittle) failure while curved portions are related to Type II (ductile) failure as discussed in the previous section. When K^* is fixed, as the brittleness number B increases from 0.001, the failure mode undergoes a transition from brittle to ductile. However, at larger values of B and for all values of K^*, curves revert back to the LEFM limit, which is given by (1) and

$$K_{IC} = \sqrt{E'(G_f + G_m)}, \quad G_m = K_m^2/E' \tag{19}$$

Here the composite elastic modulus $E' \approx E'_m$ is assumed, which is quite accurate for low fiber volume fraction cases (e.g., several percent). It can be shown that this LEFM limit for σ_N/σ_0 is given by

$$\frac{\sigma_N}{\sigma_0} = \left(\pi(K^*)^2 + \frac{8}{3\pi}\right)^{1/2} f^{-1}\left(\frac{a_0}{b}\right)\left(\frac{b}{l_{ch}}\right)^{-1/2} \tag{20}$$

While the structural brittleness at large brittleness number has been well recognized, the brittleness at small B revealed in this study is due to the inadequate FPZ development as limited by small structural size b if other parameters are fixed.

On the other hand, as K^* decreases from 0.5–0.01, meaning fiber bridging effect is getting stronger, all the curves tend to collapse into a master curve (the bottom ones in Fig. 5(a)–(h)). Further decrease in K^* makes essentially no difference. This implies that when crack bridging is strong enough or the fracture energy is sufficiently high, the structural size-effect is governed by the fundamental fiber and interface properties and the matrix toughness becomes irrelevant. In the case of ductile failure, the limiting value of σ_N/σ_0 as $b \to 0$ or $l_{ch} \to \infty$ is given by a plastic hinge analysis (Carpinteri, 1989). Referring to Fig. 6, it is readily shown that

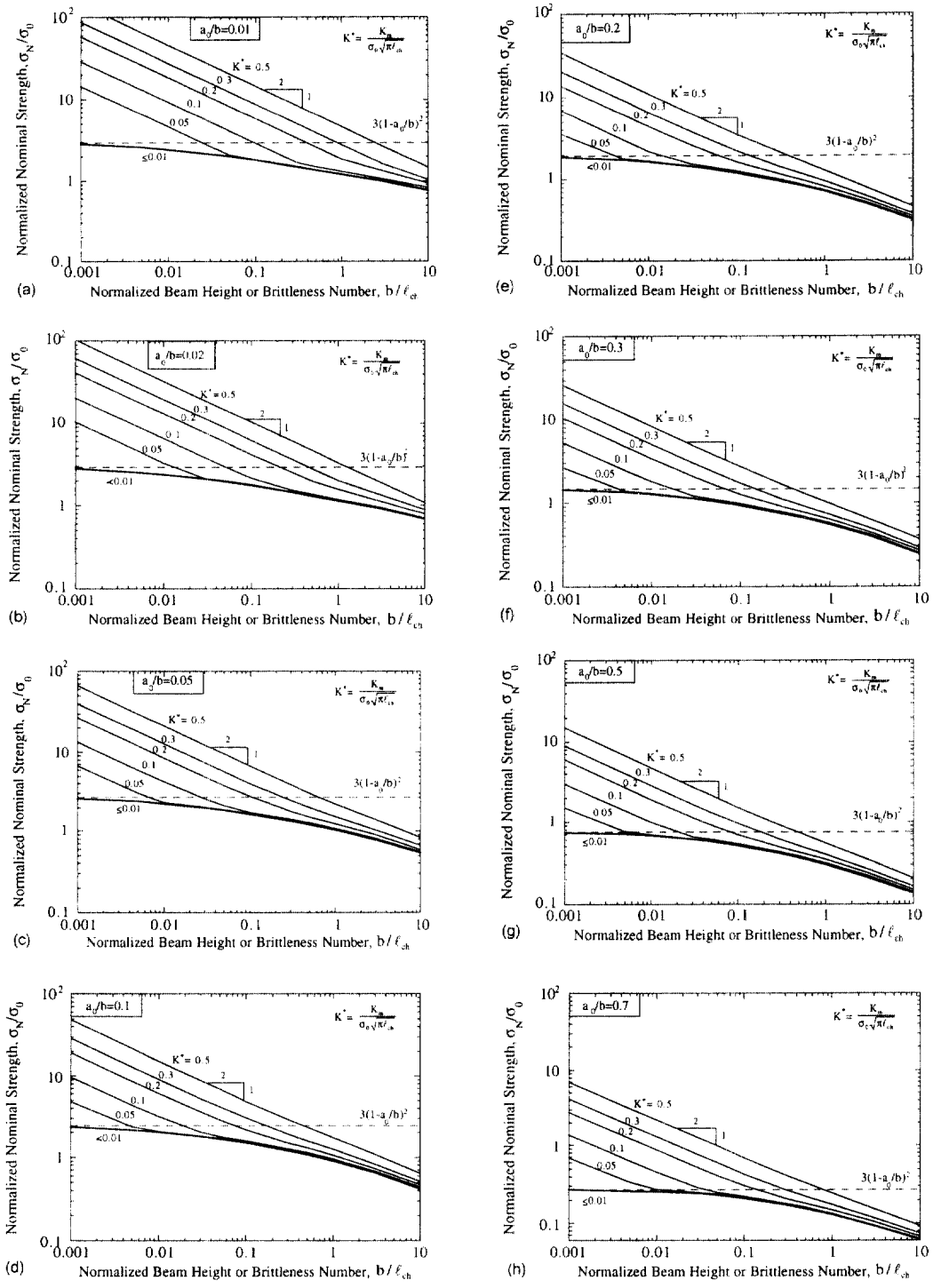

Fig. 5. The generic size-effect law for three-point bending FRC beams: (a) $a_0/b = 0.01$; (b) $a_0/b = 0.02$; (c) $a_0/b = 0.05$; (d) $a_0/b = 0.1$; (e) $a_0/b = 0.2$; (f) $a_0/b = 0.3$; (g) $a_0/b = 0.5$; and (h) $a_0/b = 0.7$.

$$\sigma_N/\sigma_0 = 3(1-a_0/b)^2, \quad \text{as } B \to 0 \tag{21}$$

and this "fully yielding" limit is shown as a dashed horizontal line in each of the plots shown in Fig. 5.

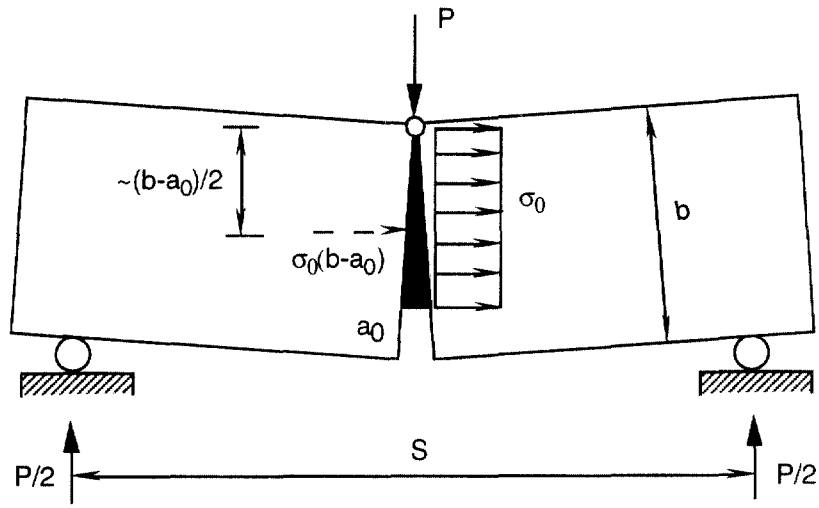

Fig. 6. Stress distribution and force balance in a plastic hinge analysis as b approaches zero.

It should be also pointed out that with all the material and geometric parameters other than the beam height b fixed, the transition from brittle to ductile failure for small a_0/b cases occurs at larger b's than for large a_0/b cases (e.g., $a_0/b = 0.02$ vs $a_0/b = 0.2$). This is due to the fact that smaller initial notch requires higher first cracking load and a larger subsequent FPZ to develop in order to realize Type II behavior. Alternatively, a smaller a_0/b is equivalent to a larger K_m.

Figure 7 shows the predicted nominal strength for ductile FRC beams ($K^* \leqslant 0.01$) as a function of the brittleness number B and initial notch a_0/b.

As an example, Fig. 8 shows the comparison among a 2% polyethylene (Spectra 900) FRC, ordinary concrete and mortar (Bazant and Pfeiffer, 1987) as well as high strength concrete (HSC) (Duda and Konig, 1990) in terms of size-effect in real dimensions. The MOR values for 2% Spectra 900 FRC beams (unnotched) are taken from Maalej and Li

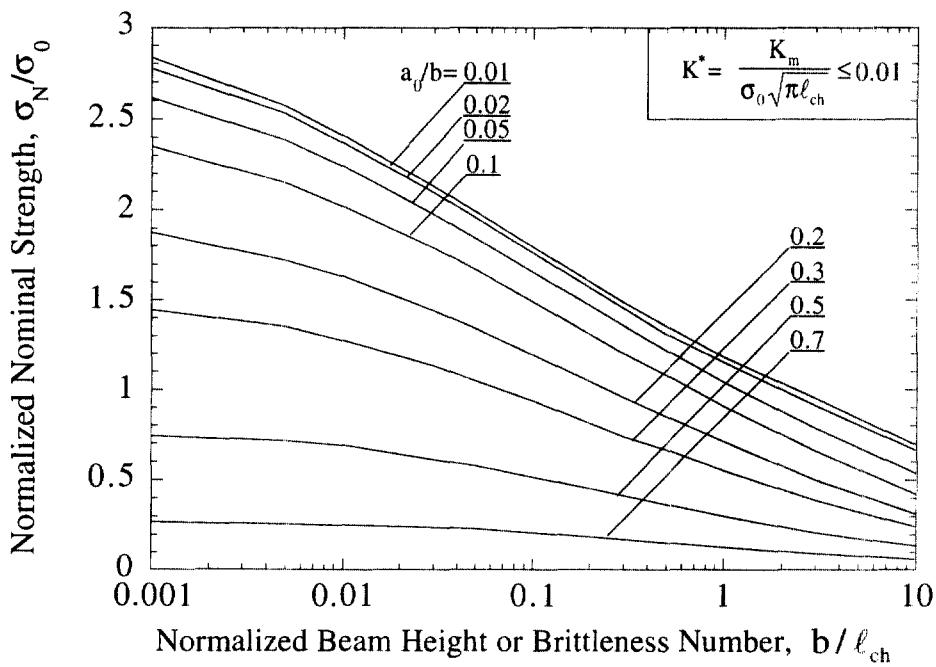

Fig. 7. Predicted nominal strength for ductile FRC beams ($K^* \leqslant 0.01$) as a function of the brittleness number B and initial notch a_0/b.

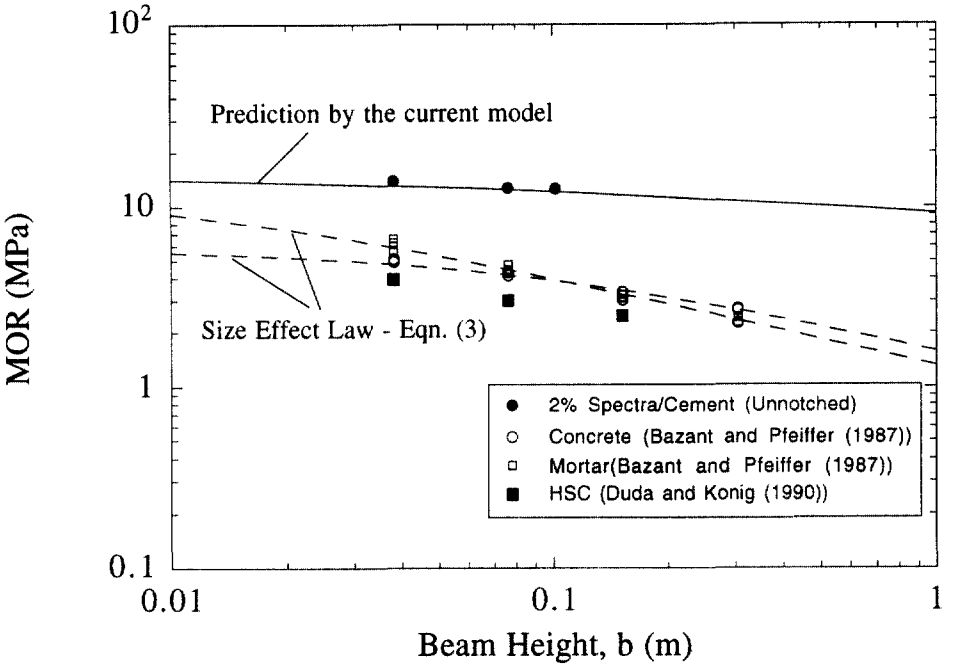

Fig. 8. Comparison of size-effect in Spectra FRC, concrete, mortar and HSC in real dimensions.

(1994), Li *et al.* (1996) and Lim *et al.* (1997). The parameters used for the prediction are $\tau = 0.75$ MPa, $g = 2$, $L_f = 12.7$ mm, $d_f = 38$ μm and $a_0/b = 0.02$. The results from the Size-Effect Law [eqn (3)] are also included in Fig. 8 (for concrete: $G_f = 37$ J/m^2, $c_f = 13.4$ mm; for mortar: $G_f = 20$ J/m^2, $c_f = 1.9$ mm (Bazant and Kazemi, 1990)). It can be seen from Fig. 8 that Spectra 900 FRC shows much less size-effect than ordinary concrete, mortar and HSC within the practical range of real sizes.

Figure 9 shows the bridging stress distribution as the bridging zone develops for $K^* \leqslant 0.01$ and for different brittleness numbers. In all four cases, the fracture process zone remains attached to the initial notch tip when MOR is reached.

Size-effect on R-*curve behavior*

The fracture resistance curve (R-curve) due to fiber bridging can be evaluated by (Rice, 1968)

$$G_R(a) = \int_0^{\delta_t} \sigma_B(\delta)\, d\delta \tag{22}$$

where δ_t is the crack opening at the tip of a FPZ, which can be computed in the numerical simulation for given values of a. Plotted in Fig. 10 are the R-curves corresponding to various brittleness numbers for $K^* \leqslant 0.01$ and (a) $a_0/b = 0.02$ and (b) $a_0/b = 0.2$. It is not surprising to see that only for very large brittleness numbers the material fracture energy G_f (due to fiber bridging) can be fully utilized. The fact that with the laboratory specimens, the measured fracture energy G_c (at maximum load) is always lower than the true one has been found by many researchers (e.g., Li *et al.*, 1987; Li and Liang, 1986; Shah, 1984).

The shape of the curves are also quite different for different brittleness numbers. For large brittleness numbers, the R-curves tend to concave downwards and saturate after certain amount of crack extension, which is the typical, familiar shape of R-curves. For small brittleness numbers, however, the R-curves tend to concave upwards. This unusual behavior has been observed in FRCs with large l_{ch} (e.g., asbestos/cellulose cement mortar (Mai, 1991)) and in ceramic composites with small b (e.g., Al/Al_2O_3 composite (Zok, 1991)). These computed R-curves may be useful to estimate the real material fracture energy

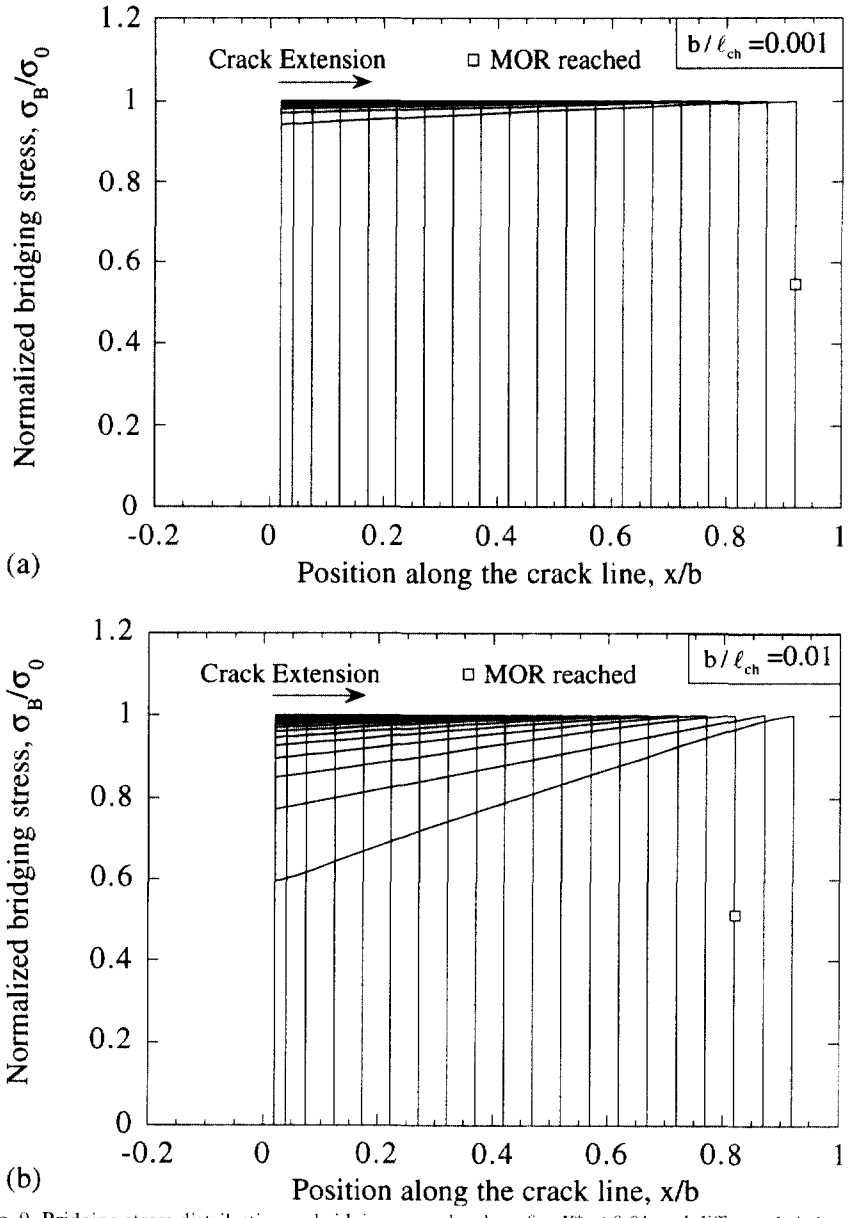

Fig. 9. Bridging stress distribution as bridging zone develops for $K^* \leqslant 0.01$ and different brittleness numbers: (a) $b/l_{ch} = 0.001$; (b) $b/l_{ch} = 0.01$; (c) $b/l_{ch} = 0.1$; and (d) $b/l_{ch} = 1.0$.

G_f from G_c data measured using small-size specimens. Figure 11 shows the prediction of the ratio between measured fracture energy G_c and material fracture energy G_f if a notched three-point bending FRC beam is to be used ($a_0/b = 0.2$). This corresponds to the suggested technique by Bazant and Pfeiffer (1987) for measurement of fracture energy of concrete using geometrically similar specimens.

Critical crack length

The critical crack length a_c is defined as the total crack length including the initial notch and the bridging zone length when MOR is reached. This quantity sometimes is very important if a simplified load-carrying capacity design method is to be used, which is usually based on the stress distribution along the critical cross-section of a FRC beam. For example, a recent Japanese design provision for steel-fiber-reinforced concrete (SFRC) tunnel linings assumes that $a_c/b = 0.7$ regardless of the size-effect. Since the estimated load carrying capacity based on the stress-distribution over a_c is sensitive to the critical crack

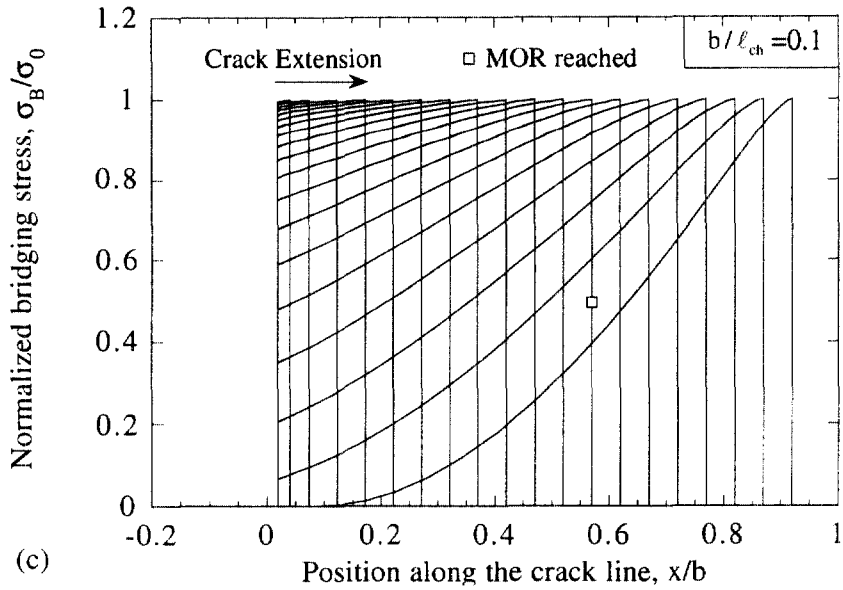

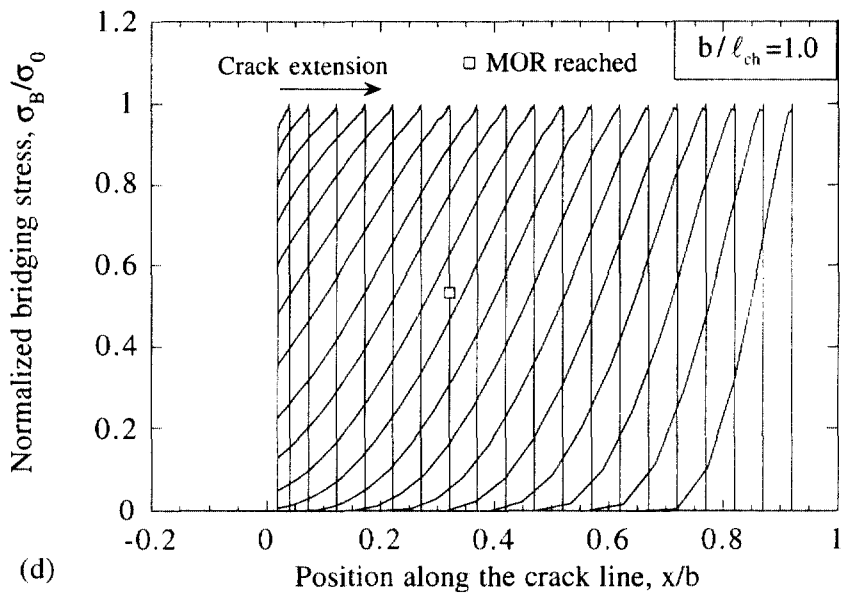

Fig. 9.—*Continued.*

length, an improper choice of a_c may lead to either over-conservative or unsafe design. This issue was addressed by Nanakorn *et al.* (1996).

Plotted in Fig. 12 is the normalized critical crack length vs brittleness number curves for $K^* \leqslant 0.01$ $a_0/b = 0.02$ and $a_0/b = 0.2$. It is obvious that the normalized critical crack length strongly depends on the structural size. Caution needs to be taken in any design practice with regard to this aspect. It should be noted that in the cases presented in Fig. 12, when the critical crack length is reached, it is fully bridged except in the initial notched portion.

CONCLUSIONS

(1) Fiber bridging with increasing fiber volume fraction V_f, interfacial bond strength τ and fiber length L_f gives rise to brittle-to-ductile transition of a FRC beam, and therefore significantly reduces structural size effect (Ref. Fig. 4 and Fig. 5).

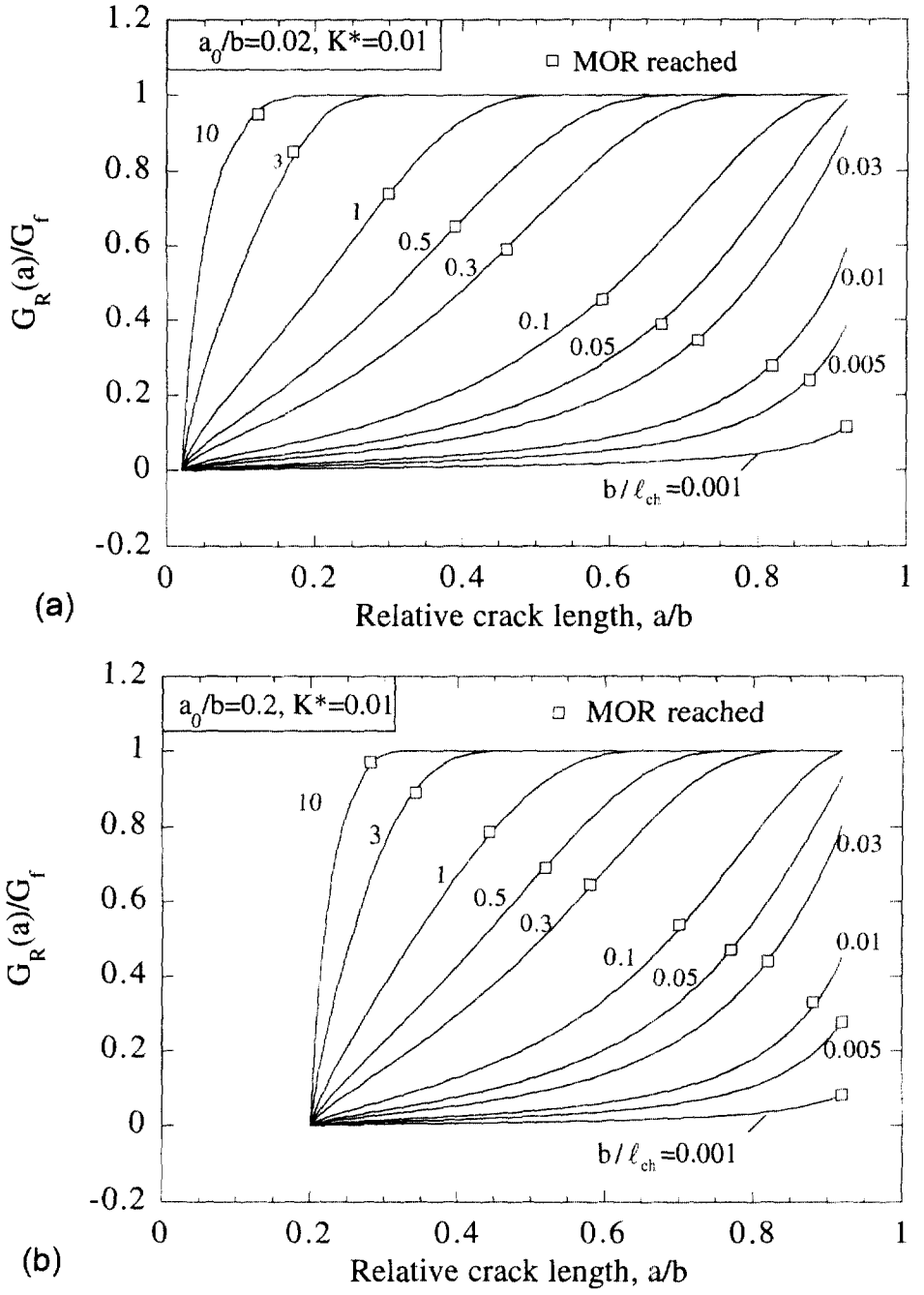

Fig. 10. *R*-curves corresponding to various brittleness numbers for $K^* \leqslant 0.01$ and (a) $a_0/b = 0.02$ and (b) $a_0/b = 0.2$.

(2) There are two types of brittle behavior of a FRC beam: (a) brittleness due to large structure size (FPZ zone relatively small; LEFM applicable) (Ref. Fig. 10), and (b) brittleness due to small structure size because of inadequate fracture process zone development as limited by the small structure size. Both are quantified as a function of the brittleness number b/l_{ch} and $(K_m/\sigma_0\sqrt{\pi l_{ch}})$ as shown in Fig. 5.

(3) When ductile failure is ensured by sufficient fiber bridging, the nominal strength of a FRC beam is dictated by fiber and interface properties. Further increase in maximum bridging stress σ_0 leads to stronger size-effect due to the decreasing material characteristic length l_{ch}. Physically, as σ_0 increases via increasing interfacial bond strength τ

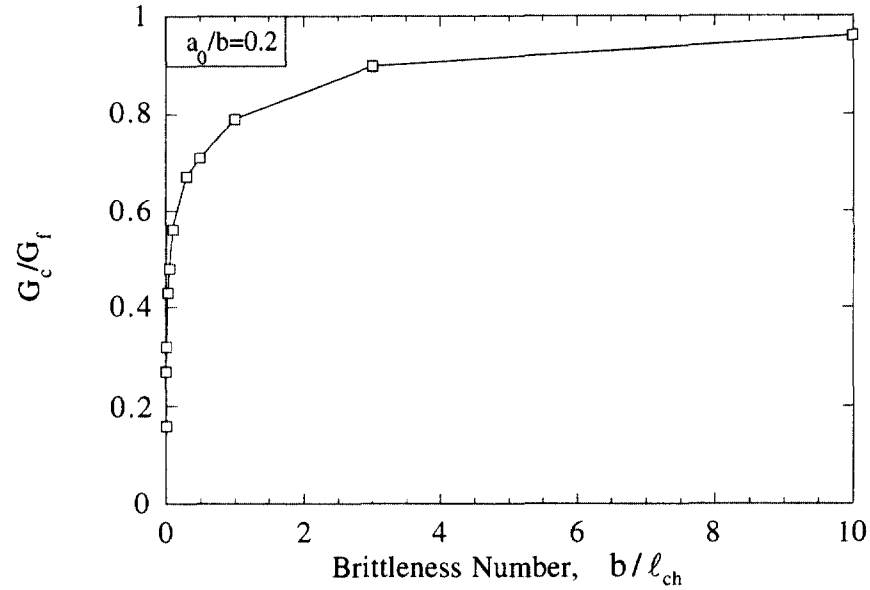

Fig. 11. Prediction of the ratio between measured fracture energy G_c and material fracture energy G_f as a function of brittleness number for $a_0/b = 0.2$.

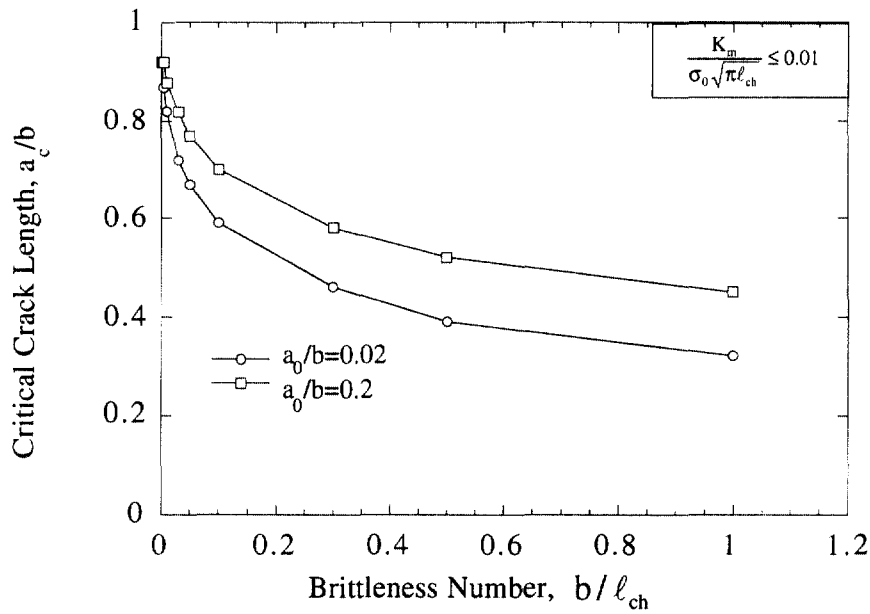

Fig. 12. Normalized critical crack length vs brittleness number curves for $K^* \leqslant 0.01$, $a_0/b = 0.02$ and $a_0/b = 0.2$.

or fiber volume fraction V_f while fiber length L_f is kept constant, the σ_B–δ curve in real dimensions will have a steeper drop, which gives rise to stronger size-effect.

(4) R-curve behavior, critical fracture energy and crack length at MOR point are strongly size-dependent. They should be carefully considered in a simplified FRC load-carrying capacity design method based on stress-distribution at the critical beam cross-section with assumed bridged crack length.

Acknowledgement—This research has been partially supported by a grant from the National Science Foundation (CMS-9601262) to the ACE-MRL at the University of Michigan.

REFERENCES

Barenblatt, G. I. (1962) The mathematical theory of equilibrium cracks in brittle fracture. *Advances in Applied Mechanics* **7,** 55–129.

Bazant, Z. P. (1984) Size effect in blunt fracture: concrete, rock, metal. *ASCE Journal of Engineering Mechanics* **110,** 4, 518–535.

Bazant, Z. P. (1987) Fracture energy of heterogeneous materials and similitude. In *Fracture of Concrete and Rock*, ed. S. P. Shah and S. E. Swartz, pp. 229–241. Springer-Verlag.

Bazant, Z. P. (1992) Size effect and brittleness of structures. In *Fracture Mechanics of Concrete Structures*, ed. Z. P. Bazant, pp. 58–67. Elsevier Applied Science.

Bazant, Z. P. and Kazemi, M. T. (1990) Determination of fracture energy, process zone length and brittleness number from size effect with application to rock and concrete. *International Journal of Fracture* **44,** 111–131.

Bazant, Z. P. and Pfeiffer, P. A. (1987) Determination of fracture energy from size effect and brittleness numbers. *ACI Materials Journal* **84,** 463–479.

Carpinteri, A. (1989) Size effects on strength, toughness and ductility. *ASCE Journal of Engineering Mechanics* **115,** 7, 1375–1392.

Chern, J.-C. and Tarng, K.-M. (1990) Size effect in fracture of steel fiber reinforced concrete. In *Micromechanics of Failure of Quasi-Brittle Materials*. International Conference, Albuquerque, U.S.A., ed. S. P. Shah, S. E. Swartz and M. L. Wang, pp. 244–53. Elsevier applied Science, London.

Cox, B. N. and Marshall, D. B. (1991) Stable and unstable solutions for bridged cracks in various specimens. *Acta Metallica Materiala* **39,** 4, 579–589.

Duda, H. and Konig, G. (1990) Stress-crack opening relation and size-effect in concrete. In *Application of Fracture Mechanics to Reinforced Concrete*, ed. A. Carpinteri, pp. 45–61. Elsevier Applied Science.

Foote, R. M. L., Mai, Y.-W. and Cotterell, B. (1986) Crack growth resistance curves in strain-softening materials. *Journal of the Mechanics and Physics of Solids* **34,** 6, 593–607.

Gettu, R. and Shah, S. P. (1994) Fracture mechanics. In *High Performance Concretes and Applications*, eds. S. P. Shah and S. H. Ahmad, pp. 161–212. Edward Arnold.

Hillerborg, A. (1983) Analysis of one single crack. *Fracture Mechanics of Concrete*, ed. F. H. Whittman, pp. 223–249. Elsevier Science Publishers, The Netherlands.

Jenq, Y. S. and Shah, S. P. (1985) A fracture toughness criterion for concrete. *Engineering Fracture Mechanics* **21,** 5, 1055–1069.

Li, V. C. (1992) Postcrack scaling relations for fiber reinforced cementitious composites. *Journal of Materials in Civil Engineering* **4,** 1, 41–57.

Li, V. C. (1995) Fiber reinforced cementitious composites in structural design/applications. *Proceedings of the 4th Japan International SAMPE Symposium*, pp. 1340–1345.

Li, V. C., Chan, C. M. and Leung, K. Y. (1987) Experimental determination of the tension-softening relations for cementitious composites. *Cem. Concr. Res.* **17,** 441–452.

Li, V. C. and Liang, E. (1986) Fracture processes in concrete and fiber reinforced cementitious composites. *ASCE Journal of Engineering Mechanics* **112,** 6, 566–585.

Li, V. C., Wang, Y. and Backer, S. (1990) Effect of inclining angle, bundling and surface treatment on synthetic fiber pull-out from a cement matrix. *Composites* **21,** 2, 132–140.

Li, V. C., Wang, Y. and Backer, S. (1991) A micromechanical model of tension-softening and bridging toughening of short random fiber reinforced brittle matrix composites. *Journal of the Mechanics and Physics of Solids* **39,** 5, 607–625.

Li, V. C., Lim, Y. M. and Chan, Y.-W. (1996) Feasibility study of a passive smart-self-healing cementitious composite. *J. Composites Engineering*, accepted.

Lim, Y. M., Wu, H. C. and Li, V. C. (1997) Development of flexural composite properties and dry shrinkage behavior of high performance fiber reinforced cementitious composites at early ages. *ACI Materials Journal*, accepted.

Lin, Z. and Li, V. C. (1997) Crack bridging in fiber reinforced cementitious composites with slip-hardening interfaces. *Journal of the Mechanics and Physics of Solids* **45,** 5, 763–787.

Maalej, M. and Li, V. C. (1994) Flexural/tensile-strength ratio in engineered cementitious composites. *Journal of Materials in Civil Engineering* **6**(4), 513–528.

Mai, Y.-W. (1991) Failure characterization of fiber-reinforced cement composites with R-curve characteristics. *Toughening Mechanisms in Quasi-Brittle Materials*, ed. S. P. Shah. NATO ASI Series E: Applied Sciences—Vol. 195, pp. 467–505. Kluwer Academic Publishers.

Morton, J. and Groves, G. W. (1976) The effect of metal wires on the fracture of a brittle matrix composite. *Journal of Materials Science* **11,** 617–622.

Nanakorn, P., Horri, H. and Matsuoka, S. (1996) A fracture mechanics-based design method for SFRC tunnel linings. *J. Materials Conc. Struct., Pavements* **30,** 221–233.

Okamura, H. and Maekawa, K. (1994) Reinforced concrete design and size effect in structural non-linearity. In *Size Effect in Concrete Structures*, ed. H. Mihashi, H. Okamura and Z. Bazant, pp. 1–24. P.E.&F.N. Spon, London.

Rice, J. R. (1968) Mathematical analysis in the mechanics of fracture. *Fracture an Advanced Treatise*, ed. H. Liebowitz, **2,** 191–311. Academic Press, New York.

Shah, S. P. (1984) Dependence of concrete fracture toughness on specimen geometry and on composition. *Fracture Mechanics of Concrete: Material Characterization and Testing*, ed. A. Carpinteri and A. R. Ingraffea, pp. 111–135. Martinus Nijhoff Publishers.

Tada, H., Paris, P. C. and Irwin, G. (1985) *The Stress Analysis of Cracks Handbook*, 2nd edn. Paris Prod. Inc., St Louis, Missouri.

Wang, Y., Li, V. C. and Backer, S. (1991) Tensile failure mechanisms in synthetic fiber-reinforced mortar. *Journal of Materials Science* **26,** 6565–6575.

Zok, F. (1991) The fracture resistance of brittle matrix composites. *Toughening Mechanisms in Quasi-Brittle Materials*, ed. S. P. Shah. NATO ASI Series E: Applied Sciences—Vol. 195, pp. 467–505. Kluwer Academic Publishers.

APPENDIX

The weight function in (4) can be found in Tada *et al.* as follows

$$G(x, a, b) = \frac{1}{\sqrt{\pi a}} \frac{h_1(x/a, a/b)}{(1-x^2/a^2)^{1/2}} \tag{A1}$$

where

$$h_1(x/a, a/w) = \frac{g(x/a, a/b)}{(1-a/b)^{3/2}} \tag{A2}$$

with $g(x/a, a/b)$ is defined by

$$\begin{aligned}
g(r, s) &= g_1(s) + r g_2(s) + r^2 g_3(s) + r^3 g_4(s) \\
g_1(s) &= 0.46 + 3.06s + 0.84(1-s)^3 + 0.66s^2(1-s)^2 \\
g_2(s) &= -3.52s^2 \\
g_3(s) &= 6.17 - 28.22s + 34.54s^2 - 14.39s^3 - (1-s)^{3/2} - 5.88(1-s)^5 - 2.64s^2(1-s)^2 \\
g_4(s) &= -6.63 + 25.16s - 31.04s^2 + 14.41s^3 + 2(1-s)^{3/2} + 5.04(1-s)^3 + 1.98s^2(1-s)^2
\end{aligned} \tag{A3}$$